Applied Catalysis B: Environmental 138–139 (2013) 175–183

Contents lists available at SciVerse ScienceDirect

Applied Catalysis B: Environmental

journal homepage: www.elsevier.com/locate/apcatb

A facile approach to ZnO/CdS nanoarrays and their photocatalytic and photoelectrochemical properties

Chunmei Li[a,1], Taha Ahmed[a,1], Mingguo Ma[b], Tomas Edvinsson[a], Jiefang Zhu[a,*]

[a] Department of Chemistry, Ångström Laboratory, Uppsala University, Uppsala 75121, Sweden
[b] Institute of Biomass Chemistry and Technology, College of Materials Science and Technology, Beijing Forestry University, Beijing 100083, PR China

ARTICLE INFO

Article history:
Received 21 August 2012
Received in revised form 14 February 2013
Accepted 18 February 2013
Available online 28 February 2013

Keywords:
ZnO
CdS
Nanoarray
Photocatalysis
Photoelectrochemistry

ABSTRACT

ZnO nanorods were successfully deposited on Transparent Conductive Oxide (TCO) glass by electrochemical deposition, during which initial pulse potential proves important for the fast nucleation and even distribution of ZnO. CdS nanoparticles were coated outside the as-prepared ZnO nanorods by chemical-bath deposition forming ZnO/CdS nanoarrays. The nanoarrays were characterized by X-ray diffraction (XRD), Raman spectroscopy, scanning electron microscopy (SEM), energy dispersive spectroscopy (EDS), ultraviolet–visible (UV–vis) spectroscopy, and photoelectrochemistry. The short-circuit current density (J_{sc}) of some ZnO/CdS sample showed over 3.3 mA/cm^2 under solar-simulated illumination. The ZnO/CdS nanoarrays showed promising photocatalytic activity with respect to the degradation of Eriochrome Black T (EBT). The relatively high photoelectrochemical properties and photocatalytic performance under visible light irradiation can be ascribed to the enhanced visible light harvest from CdS and charge separation by the coupling of the semiconductors. The combination of electrodeposition and chemical-bath deposition can provide a simple and facile approach to the fabrication of one-dimensional nanocomposites.

1. Introduction

ZnO has a large application potential in photocatalysis and photovoltaic cell, due to its diverse physical properties and finely tunable preparation. ZnO is a direct-bandgap semiconductor, and has a wide bandgap of 3.3 eV. It has similar conduction and valence positions as anatase TiO_2, and therefore has been frequently considered as an alternative to TiO_2 for photocatalytic and photovoltaic applications. Compared to anatase TiO_2, the electron mobility is higher in ZnO, especially in single-crystalline ZnO [1,2]. It is well known that the materials properties depend largely on the way of synthesizing them. For synthesis of ZnO nanomaterials, various methods have been developed, including gas-phase methods (e.g. metal-organic chemical vapor deposition (MOCVD), vapor phase epitaxy (VPE), and pulsed-laser deposition (PLD)) and solution-phase methods (e.g. chemical-bath deposition, electrochemical deposition, and solvothermal methods) [3]. For photovoltaic and photoelectrochemical applications, it is important to form ZnO directly on conductive substrate without destroying the microstructure. Immobilization of photocatalysts is also a practical issue, considering industrialization. Among various synthetic strategies, electrodeposition has the advantage of being controllable, simple, inexpensive and suitable for large-scale production, and it can be applied in thin film materials fabrication on conductive substrates with arbitrarily shaped surfaces. In particular, it can be one of the most efficient methods in controlling the growth of 1D semiconductor nanostructures such as nanorods. 1D nanostructures can efficiently transport electrical carriers, and can thus be considered as the ideal building blocks to construct a new generation of nanoscale electronic, photonic and photoelectronic devices [4]. The nanorod is the most basic and common morphology among 1D nanostructures. Although there have been many reports on the electrodeposition of ZnO nanorods, in most cases additives (including templates, capping reagents, etc.) [5–10], precoated metal layers [11] or single-crystalline substrates [12,13] have been used to control nanorod growth during ZnO electrodepositions. Here we instead focus on using initial voltage pulse. ZnO cannot absorb and utilize visible light due to its broad bandgap [14] and in order to overcome this inherent drawback, narrow bandgap semiconductors (α-Fe_2O_3, CdS, etc.) have been used to modify ZnO [15]. Among these narrow bandgap semiconductors, CdS has suitable valence and conduction band edges well-matching those of ZnO for the separation of photogenerated charge carriers. Furthermore, CdS itself is also a visible-light responsive photocatalyst and a photoanode material. Therefore, the idea coupling CdS with ZnO has been continuously attracting research interest [3,16–19].

* Corresponding author. Tel.: +46 18 471 3722; fax: +46 18 153548.
E-mail addresses: jiefang.zhu@kemi.uu.se, jiefangzhu@hotmail.com (J. Zhu).
[1] These authors contributed equally to this work.

0926-3373/$ – see front matter © 2013 Elsevier B.V. All rights reserved.
http://dx.doi.org/10.1016/j.apcatb.2013.02.042

In this study, we have applied initial pulse potential in the electrodeposition of ZnO nanorods on fluorine doped tin oxide (FTO) glass. It turns out that the initial pulse potential is an important starting step in the formation of evenly distributed ZnO seeds on FTO glass. In order to improve the photocatalytic and photoelectrochemical performances of these ZnO nanorods under visible-light irradiation, CdS nanoparticles were coated outside ZnO nanorods to construct ZnO/CdS nanoarrays, which gave enhanced photocatalytic and photoelectrochemical performances under visible-light irradiation. This can be assigned to the high light-harvesting efficiency of the nanoarray structure, the charge carrier separation between CdS and ZnO, and the fast electron transportation in the ZnO nanorods.

2. Experimental

2.1. Materials

All chemicals were of reagent grade, purchased from Sigma–Aldrich and used without further purification. Ultra-pure water (18 MΩ cm) was used in all solutions.

2.2. Preparation of ZnO/CdS nanoarrays

A three-electrode system was used for the electrodeposition of ZnO nanorods, including Pt as the counter electrode, a saturated calomel electrode (SCE) as the reference electrode, and FTO glass (8–10 Ω/sq, TEC8 from Pilkington) as working electrode. The electrolyte consisted of 0.1 mM $ZnCl_2$ and 0.1 M KCl dissolved in water (pH 6.2). The bath temperature was kept at 80 °C. Before deposition, the FTO glass was cleaned with ethanol, glassware detergent and diluted hydrochloric acid, and then rinsed with water. ZnO nanorods were electrodeposited in two steps. A potential of −1.3 V vs. SCE was applied for 0.1 s (voltage pulse) followed by a potential of −0.7 V vs. SCE for the deposition duration using a μAutolab Type II Potentiostat/Galvanostat. In the process of electrodeposition, oxygen was bubbled into the electrolyte with a flow rate 0.2 l/min, and the electrolyte was continuously stirred with a magnetic stirrer. ZnO is deposited cathodically, and the deposition reaction on FTO can be described by [20]

$$Zn^{2+} + ½O_2 + 2e^- \rightarrow ZnO \quad E^0 = 0.93\,V/NHE \tag{1}$$

Deposition time was 0.5 h, 1.5 h, or 3 h. For comparison, the sample was also deposited without the initial voltage pulse.

CdS nanoparticles were coated on the ZnO nanorods by chemical-bath deposition. The aqueous bath solution (pH 11.3) consisted of 2 mM $CdSO_4$, 10 mM CH_4N_2S, and 1 M $NH_{3(aq)}$. The bath temperature was thermostatically held at 60°C before immersing the substrate (ZnO nanorods on FTO). The deposition time was 3 min, 10 min, 20 min, 40 min, or 80 min. Additionally, CdS was directly deposited on FTO glass for comparison. The reaction process can be described as follows:

$$NH_3 + H_2O \leftrightarrow NH_4^+ + OH^- \tag{2}$$

$$Cd^{2+} + 4NH_3 \leftrightarrow [Cd(NH_3)_4]^{2+} \tag{3}$$

$$(NH_2)_2CS + OH^- \rightarrow CH_2N_2 + H_2O + HS^- \tag{4}$$

$$HS^- + OH^- \rightarrow S^{2-} + H_2O \tag{5}$$

$$Cd^{2+} + S^{2-} \rightarrow CdS\downarrow \tag{6}$$

$$Cd^{2+} + 2OH^- \rightarrow Cd(OH)_2\downarrow \tag{7}$$

$$Cd(OH)_2 + S^{2-} \rightarrow CdS\downarrow + 2OH^- \tag{8}$$

Ammonia dissolved in water produces equilibrium hydroxide ions (2) and forms a cadmium tetrammine complex (3). Ammonia has the roles of increasing the pH of solution as well as preventing violent cadmium hydroxide formation through coordination to the Cd^{2+} ion (3). In an alkaline solution, thiourea decomposes (4) and generates free sulfide ion (5). CdS forms through an ion-by-ion mechanism (6) and/or a hydroxide cluster mechanism (7, 8) [3].

2.3. Characterization

The crystal structure of samples was analyzed by an X-ray diffractometer (SIEMENS Diffractometer D500) with Cu Kα radiation (λ = 1.54 Å) at 45 kV and 40 mA. The Raman measurements were performed with a Renishaw micro-Raman 2000 using 10 mW from a 514 nm argon ion laser. A 50× objective lens was used which gave a laser spot within 5 μm diameter on the samples. All samples were measured with a 30 s exposure time and 10 acquisition cycles between 200 cm^{-1} and 550 cm^{-1}. Raman shift was calibrated with Si at 521 cm^{-1} before sample measurement. High-resolution scanning electron microscopy (SEM) was carried out using a LEO 1550 FEG, equipped with an INCA Energy Dispersive X-ray Spectrometer (EDX) and operated at 10 kV. The diameter distribution of ZnO nanorods and ZnO/CdS nanoarrays was counted by measuring the diameter of 200 rods or arrays per sample. Transmission electron microscopy (TEM) micrographs were taken with a Tecnai F30 transmission electron microscope (FEI Company) using an accelerating voltage of 300 kV, which was equipped with an energy dispersive X-ray spectrometer (EDX) operated at 40 kV. For TEM observations, the sample powders were scratched from the FTO substrate, and dispersed in ethanol by ultrasonic irradiation, and a drop of the suspension was placed onto a carbon-coated copper grid (Ted Pella, US). The deposit was dried in air prior to observation. Transmittance and reflectance spectra of samples were measured using a Lambda 900 UV/VIS/NIR spectrophotometer (PerkinElmer instruments) equipped with an integrating sphere. Steady-state emission spectra were obtained on a Fluorolog-3 instrument (Horiba Jobin Yvon) equipped with double-grating excitation and emission monochromators and a 450 W Xe lamp as a light-source. Right-angle detection (with the substrate at 30° with respect to the incident beam) was used to minimize inner-filter effects. A 400 nm long-pass filter was placed after the sample to reduce second-order diffraction by the excitation monochromator (for λ_{exc} = 350 nm and 375 nm).

2.4. Photoelectrochemical and photocatalytic performance testing

The current-voltage measurement was carried out by a three-electrode potentiostat (CH Instruments 760 C). Pt, Ag/AgCl and the sample were used as the counter electrode, the reference electrode and the working electrode, respectively. 1 M Na_2S solution (pH 13.6) was used as the electrolyte. The sample side of the working electrode was illuminated with solar-simulated light using an Oriel 300 W Xe-lamp fitted with an AM1.5G filter. The light intensity was adjusted to 1 kW/m^2 in the full wavelength region with a calibrated Si-diode as well as with a pyranometer.

The photocatalytic performance of the samples was quantified by the degradation of Eriochrome Black T (EBT) using a blue LED lamp (50 W, Allray Inc) with a peak emission at 450 nm and FWHM of 20 nm. Sample films with an effective size of 1 cm × 1 cm were horizontally immersed in 30 ml of 10 mg/L EBT solution in a 50 ml beaker. The illumination intensity at the sample level (0.4 W/cm^2) was measured with a thermal power sensor (Coherent 300 Power Meter). The EBT solution with immersed sample was stirred in the dark for half an hour to allow EBT equilibrium adsorption on the sample. Control experiments with only catalytic sample or only light irradiation showed little degradation of EBT. During a photocatalytic experiment, a small volume of the clear supernatant

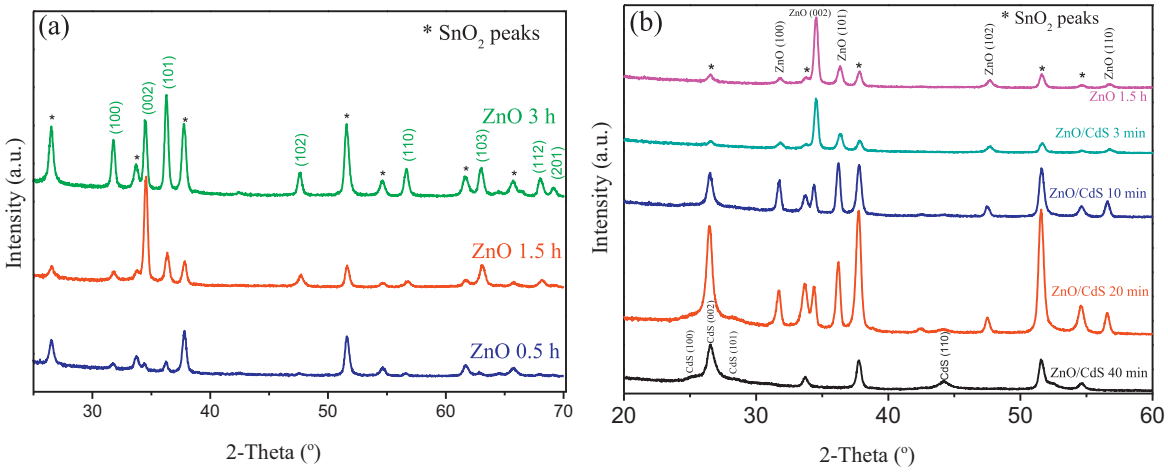

Fig. 1. XRD patterns of (a) ZnO electrodeposited for different time (0.5 h, 1.5 h and 3 h) and (b) ZnO/CdS with different deposition time of CdS (3 min, 10 min, 20 min and 40 min) and their ZnO nanorod substrate (ZnO 1.5 h).

solution was extracted every 30 min and analyzed by a UV–vis spectrophotometer (Ocean Optics, HR2000). The degradation of EBT was determined by tracking the peak absorbance around 550 nm.

3. Results and discussion

3.1. X-ray diffraction (XRD)

Fig. 1a shows the XRD patterns of electrodeposited ZnO films, which reveals that all ZnO samples have a hexagonal wurtzite structure (JCPDS No. 36-1451). For the sample with 1.5 h deposition, the sharp and strong (0 0 2) peak in the diffractogram can be explained by a preferential growth oriented along the [0 0 0 1] direction (normal to (0 0 2) plane). Growth along the [0 0 0 1] direction is more thermodynamically favorable as the surface energy is higher for the polar surfaces perpendicular to it. The intensity of the (0 0 2) plane increases with increasing deposition time from 0.5 h to 1.5 h, but then decreases with further deposition to 3 h. This might be due to the pH change during the electrodeposition of ZnO. The pH of the electrolyte decreased from 6.1 to 4.7 after 1.5 h deposition process, which is likely to etch the ZnO along [0 0 0 1] direction. It should be noted that the slight etching of ZnO along [0 0 0 1] axis does not have to mean a decrease of the total quantity of ZnO deposited on FTO glass. This is supported by our later SEM analysis. Considering the sharp (0 0 2) peak and strong orientation achieved in the ZnO with 1.5 h electrodeposition, this sample was selected as the basis for CdS coating.

It is well known that CdS can exist in either a stable hexagonal phase or a meta-stable cubic phase, and the final phase of deposited CdS strongly depends on the chemical-bath deposition mechanism and the type of substrate [21–23]. As shown in Fig. 1b, CdS peaks show up after 20 min chemical-bath deposition of CdS on ZnO film. With increasing CdS deposition time, the intensities of the CdS peaks increase. This indicates that there is a gradual improvement in crystalline quantity and/or quality of CdS with longer chemical-bath deposition time. The sample with 40 min CdS deposition shows peaks at 2θ ~25.0°, ~26.5°, ~28.3° and ~43.9°, which correspond to the (1 0 0), (0 0 2), (1 0 1) and (1 1 0) planes of the hexagonal CdS structure (JCPDS No. 41-1049). Since the (1 1 1) and (2 2 0) peaks of cubic CdS (JCPDS No. 01-89-0440) lie at very close proximity to the (0 0 2) and (1 1 0) peaks of hexagonal CdS, it is difficult to claim only from XRD that there is no cubic CdS present. Fig. 1b also shows that the intensity of ZnO peaks decreases with continuing the chemical-bath deposition of CdS after a certain time, especially for (0 0 2) plane, which almost disappears after 40 min deposition of CdS. This might be due to the etching effect on ZnO, which has been observed before [3]. These observations are in good agreement with the results of Raman spectroscopy and EDS presented below.

3.2. Raman spectroscopy

Fig. 2a shows the Raman spectra of electrodeposited ZnO films. The peak of ZnO at ~441 cm^{-1}, corresponding to the non-polar optical phonon E_2 (high) mode of wurtzite ZnO [24,25], shows up after deposition for 1.5 h and increases in intensity after 3 h deposition, showing clear signs of more ZnO with longer deposition time. Fig. 2b shows the Raman spectra of ZnO/CdS composites with different CdS deposition time. The peak at ~309 cm^{-1} pertains to the first-order longitudinal-optical (1LO) phonons of hexagonal CdS [26]. Since cubic CdS would show a peak at ~243 cm^{-1} [27], which was not observed (see Fig. 2b), the Raman spectra clear up any remaining doubt from the XRD data that the CdS in ZnO/CdS composites only exists in hexagonal structure. The formation of hexagonal CdS might thus be ascribed to the influence of the ZnO substrate, although the cubic phase is more stable at room temperature [19]. The intensity of CdS peaks increases with increasing CdS deposition time (within the studied time range), which indicates that more and more CdS is deposited. An interesting observation is that pure CdS deposited directly on FTO glass by chemical bath for 2 h has weaker Raman signals than CdS deposited on ZnO for 20 min, which indicates that the deposition and growth of CdS strongly depend on the substrate and the surface area. In Fig. 2(b), the signals of ZnO are missing in all spectra of ZnO/CdS composites, apart from the sample with the shortest CdS deposition time (3 min). This indicates a large coverage of CdS, shielding the deeper-laying ZnO from Raman response. In addition, the Raman resonance of CdS can be enhanced due to the electronic excitation by the argon ion laser. Magnifying the Raman curve can verify the coexistence of ZnO and CdS in ZnO/CdS composites, especially for samples with short CdS deposition. In the inset of Fig. 2(b), the sample of ZnO/CdS composites with 3 min CdS deposition clearly shows two signals, namely ZnO at ~441 cm^{-1} and CdS at ~309 cm^{-1}. The intensity of ZnO peak in the spectrum is slightly lower than the one corresponding to bare ZnO. This complies with the result from XRD pattern.

3.3. Electron microscopy (EM)

The morphology and size of electrodeposited ZnO was studied by SEM. Fig. 3a shows ZnO prepared without initial voltage

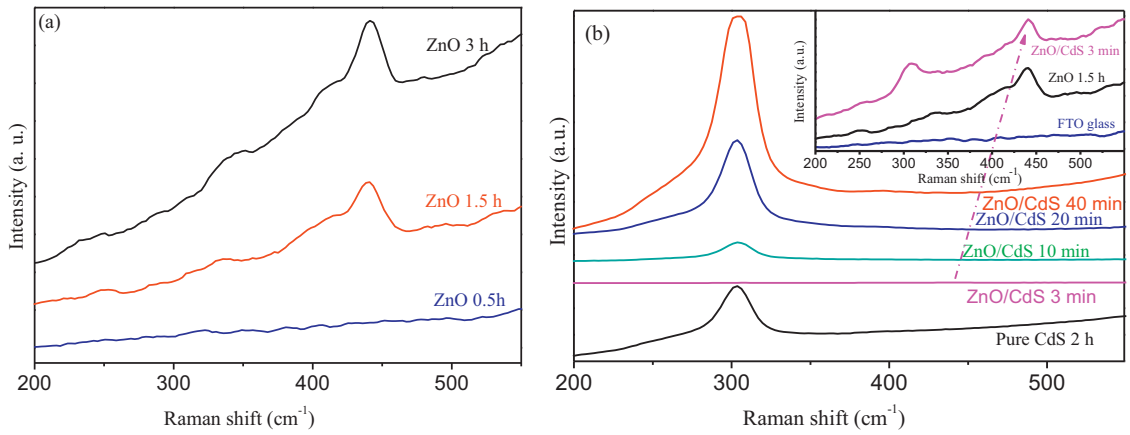

Fig. 2. Raman spectra of (a) ZnO electrodeposited for different time (0.5 h, 1.5 h and 3 h) and (b) ZnO/CdS with different deposition time of CdS (3 min, 10 min, 20 min and 40 min) and pure CdS. The inset shows the comparison between the substrate FTO glass, ZnO and ZnO/CdS.

pulse. Without an initial voltage pulse, the sample shows a heterogeneous distribution on the substrate and a low deposit density. ZnO nanorods (or blocks) grow in clusters and are short. It is well-established that when the surface energy of the substrate is much smaller than that of the deposits, the growth of isolated 3D islands is more favored. In other words, without the help of a potential voltage pulse prior to the constant-voltage electrodeposition, the ZnO would deposit preferably on the primary ZnO crystals rather than on the FTO substrate, thus forming the observed hierarchical structure. Different times and potentials were also tested for the formation of a homogeneous seed layer where 0.1 s and −1.3 V vs. SCE were found to be good enough. A shorter time leads to too low seed density, while too long time results in the formation of a continuous layer of ZnO on FTO. Fig. 3b–d demonstrates the morphology of ZnO nanorods prepared with an initial voltage pulse followed by a constant-voltage deposition of different durations. In Fig. 3b, ZnO nanorods grown for 0.5 h have lower deposition density and shorter length than those shown in Fig. 3c and d. Fig. 3c shows

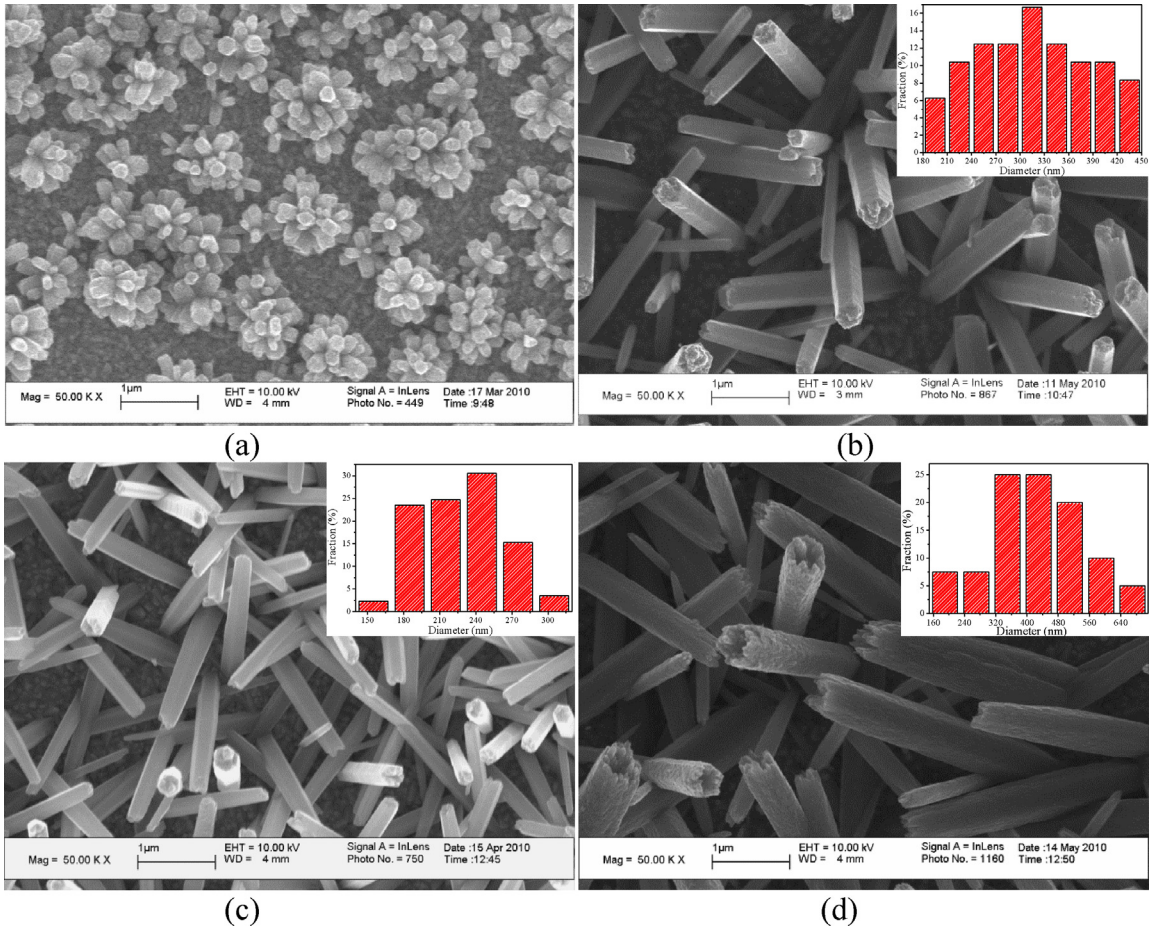

Fig. 3. SEM images of (a) ZnO by 1.5 h electrodeposition without initial pulse, and ZnO by electrodeposition with 0.1 s initial pulse for (b) 0.5 h, (c) 1.5 h, and (d) 3 h. The insets show the diameter distribution of ZnO rods.

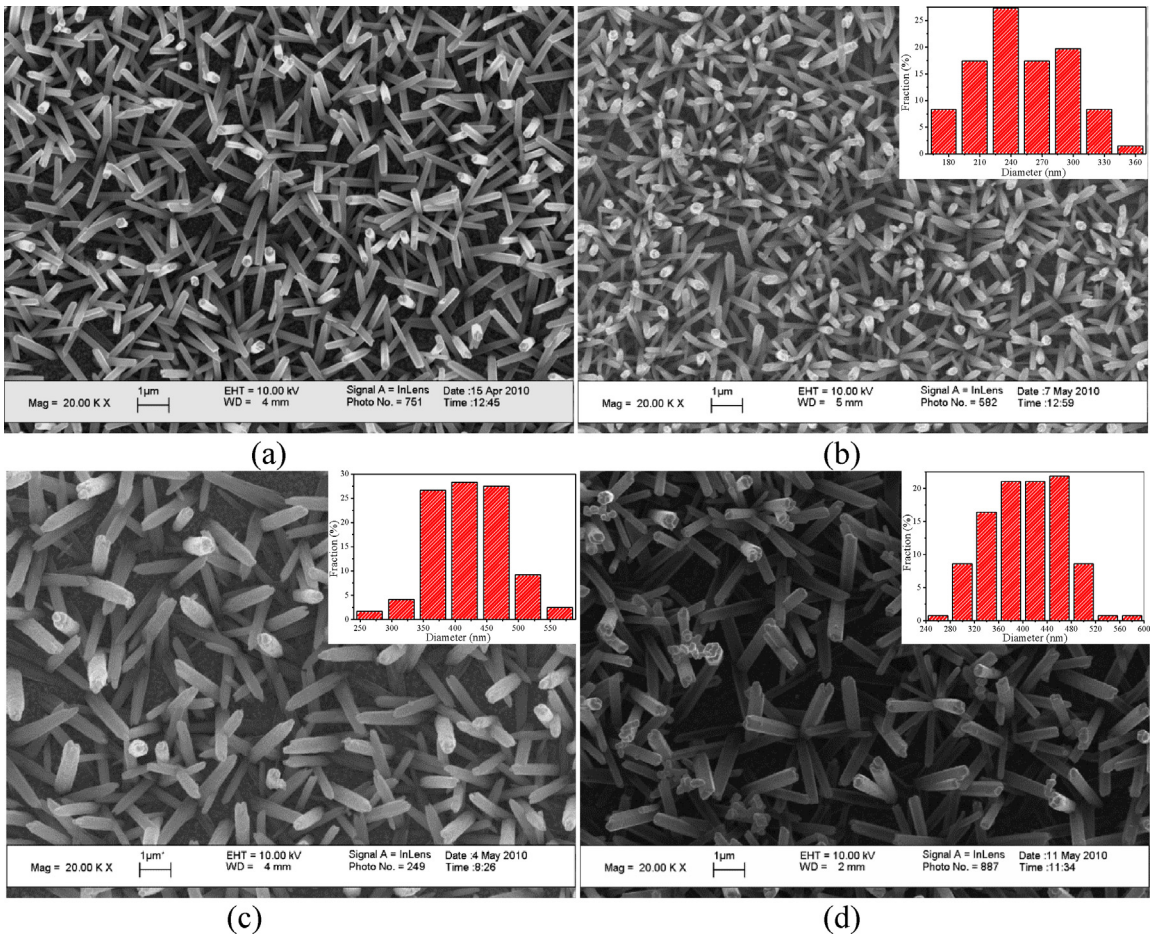

Fig. 4. SEM images of (a) ZnO by 1.5 h electrodeposition with 0.1 s initial pulse, and ZnO/CdS nanoarrays with different deposition time of CdS. (b) 3 min, (c) 20 min, and (d) 40 min. The insets show the diameter distribution of ZnO/CdS arrays.

that the ZnO nanorods electrodeposited for 1.5 h have a hexagonal cross-section and smooth walls; their length is around 2 μm, and their average diameter is around 220 nm with a narrow diameter distribution as shown in the inset. Longer deposition time (Fig. 3d) leads to larger diameters (~400 nm) and a broader diameter distribution (about 500 nm span) of ZnO nanorods than those in Fig. 3b and c. In contrast to the samples from shorter depositions, the ZnO nanorods in Fig. 3d have rough walls and ends. This may be ascribed to an etching effect during the long-time deposition. From the high-magnification SEM image (not shown here), the etching process seems to start from the center of the end and then slowly progress downwards. This observation is in agreement with the result from XRD in this work and other work [10]. From the presented SEM micrographs it can be concluded that initial voltage pulse is very important for the fast nucleation of ZnO on FTO glass. ZnO rods deposited for 1.5 h with initial voltage pulse show high density, long length, small diameter, narrow size distribution, and smooth surface; therefore this sample was chosen to be the substrate for subsequent chemical-bath deposition of CdS.

Fig. 4 shows the change of ZnO/CdS nanoarrays with different CdS deposition time. Fig. 4b shows that the sample with 3 min CdS deposition does not change its morphology to large degree compared to its substrate with ZnO nanorods (shown in Figs. 3c and 4a). The average diameter of ZnO/CdS nanoarrays in Fig. 4b is around 250 nm, which are a little larger than the substrate ZnO nanorods (see Figs. 3c and 4a). In Fig. 4c, the average diameter of ZnO/CdS nanoarrays with 20 min CdS deposition increases to 410 nm with a broader size distribution, compared to its ZnO substrate. This naturally follows from the larger amount of CdS nanoparticles deposited with longer deposition time. The cross-section of ZnO/CdS nanoarrays gradually turns from hexagonal to circular, due to the random deposition of CdS particles. In Fig. 4d, the diameter and size distribution of ZnO/CdS nanoarrays do not change significantly, compared to those in Fig. 4c. However, a few separated CdS clusters start to appear with the longer CdS deposition time, as also analyzed by EDX.

EDX analyzes the elemental compositions of prepared samples. The general composition of all the samples can be described as a combination of ZnO, CdS, and SnO_2 (the main component of FTO glass). The relative contents of Zn and O decrease with increasing CdS deposition time, while the relative contents of Cd and S increase. This is consistent with the results of XRD and Raman spectroscopy.

To confirm the existence of CdS nanoparticles, prepared nanoarrays were analyzed by TEM. Bare ZnO nanorods feature smooth surfaces and flat ends (Fig. 5a). CdS nanoparticles form a dense, even layer on the ZnO nanorods (Fig. 5b). The end of the nanorod is no longer flat, probably due to the etching effect during CdS deposition. Fig. 5c, shows that the CdS nanoparticles are about 20 nm in diameter and of polyhedral shape. We performed EDX measurements at the edge (shell) and centre (core) of a ZnO/CdS nanorod, by focusing the electron beam and centering it over each area. All EDX peaks could be assigned to elements in the sample, except C and Fe/Co, which stem from the carbon support and the microscope column, respectively. At the shell of the coated nanorod, we could clearly observe both the K-line of sulfur (S KL_3 2.31 keV, and the

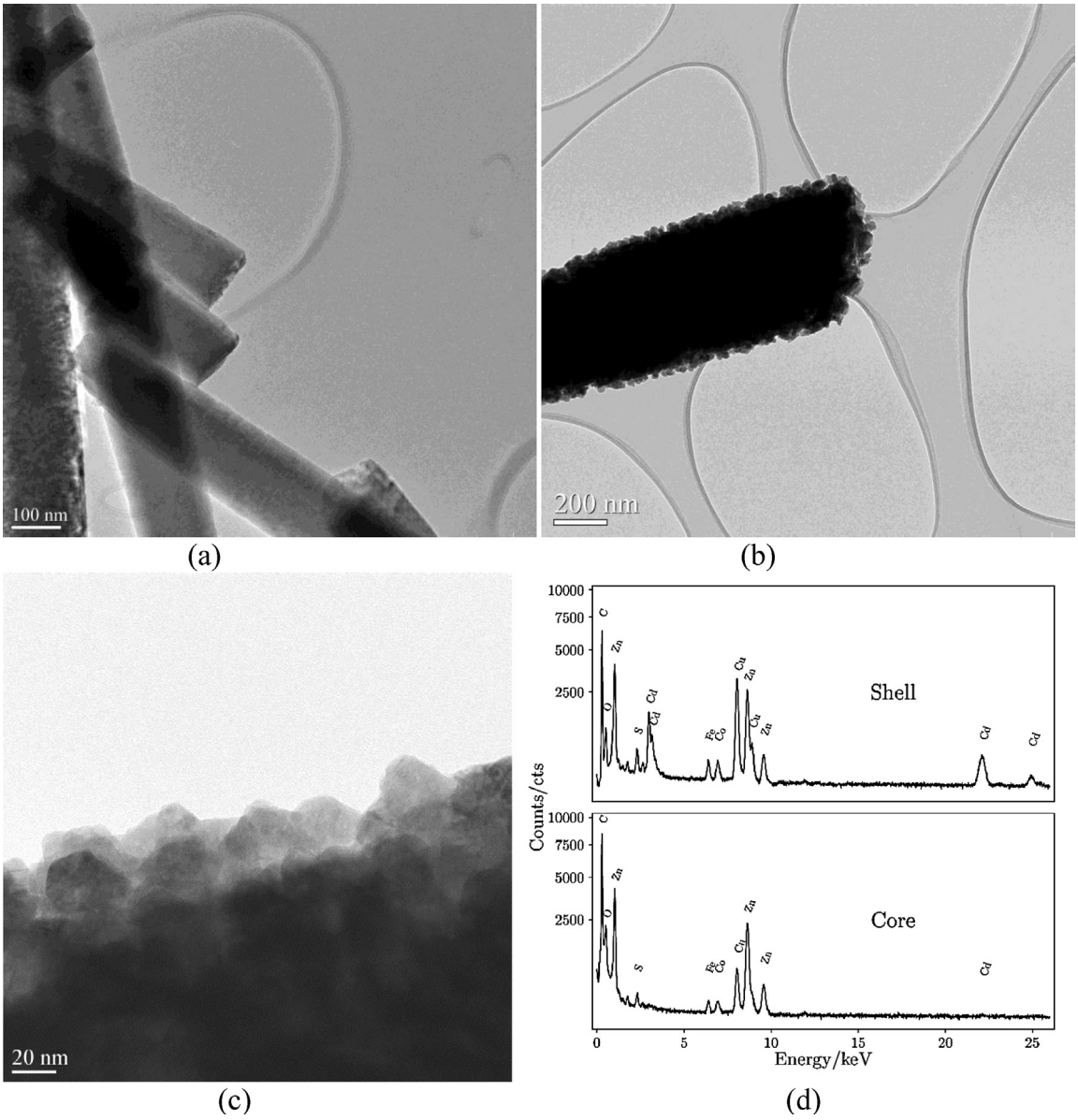

Fig. 5. TEM images of (a) ZnO by 1.5 h electrodeposition with 0.1 s initial pulse, (b) a ZnO/CdS nanoarray, and (c) an edge section of a ZnO/CdS nanoarray. (d) EDX spectra of core and shell parts of a ZnO/CdS nanoarray.

K- (Cd KL_2 22.13 keV and Cd KL_3 24.95 keV) and L-lines (Cd L_2M_1 2.99 keV and Cd L_3M_5 3.16 keV) of cadmium. The calculated atomic ratio of Zn to Cd is 17.5 based on K-lines and 15.0 based on L-lines. At the core of the nanorod, the K-line of sulfur is less intense than at the shell. The K-line of cadmium is also less intense than at the shell, and the Cd L-lines are no longer observable. This is in line with what we would expect based on the relatively low concentration of CdS at the centre of the coated nanorod. The EDX observations support our notion that the CdS is deposited like a sheath around ZnO nanorods.

3.4. Ultraviolet–visible spectroscopy (UV–vis) and photoluminescence spectroscopy (PL)

The absorption spectra of prepared samples, as shown in Fig. 6a, were calculated from the transmittance (T, including forward scattering) and reflectance (R, including backward scattering) of the samples, both of which were measured using an integrating sphere. For direct bandgap semiconductors, like ZnO and CdS, the product of their absorption coefficient α and incident photon energy $h\nu$ is proportional to the square root of the energy difference between their bandgap E_g and the incident photon energy E_λ, according to Eq. (9) [28–31].

$$\alpha_\lambda h\nu \propto \left(E_\lambda - E_g\right)^{1/2} \tag{9}$$

According to the definition of absorbance A, Eq. (9) can be easily transformed to Eq. (10).

$$(Ah\nu)^2 \propto E_\lambda - E_g \tag{10}$$

Eq. (10) shows the relationship between E_λ and the easily measurable quantity A. The bandgap E_g can be ideally given by plotting A^2 against E_λ and taken when A is zero. The intercept of the linear fit on the energy axis will give a good approximation of the bandgap for this direct bandgap material, as shown in Fig. 6b.

The absorption spectrum of ZnO deposited for 1.5 h with pulse potential has an absorption edge (estimated by the curve tangent) shorter than 390 nm, while ZnO deposited for 0.5 h with pulse potential has an absorption edge shorter than 370 nm, as shown

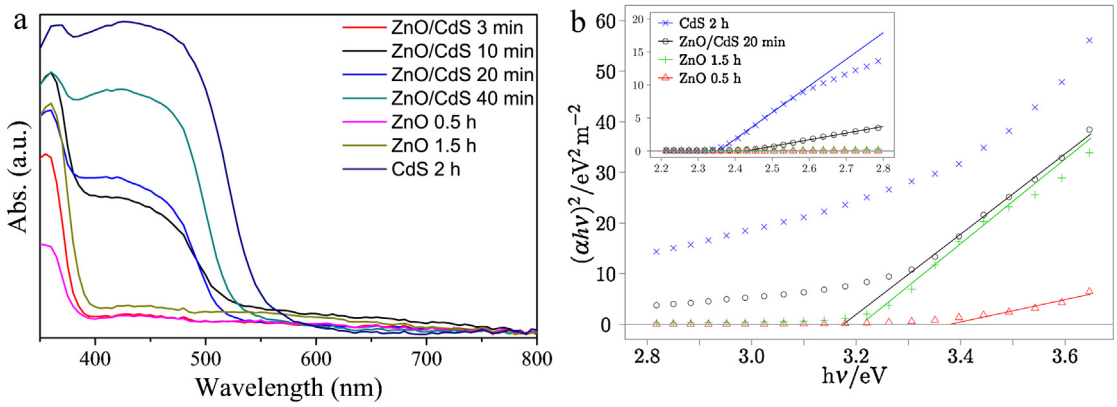

Fig. 6. (a) Absorption spectra of prepared samples and (b) the corresponding plot of $(\alpha h\nu)^2$ vs photon energy used to estimate bandgap of a direct semiconductor. The inset shows the low photon energy region used to estimate the CdS bandgap.

in Fig. 6a; their bandgaps can be estimated to 3.21 eV and 3.38 eV, respectively, as shown in Fig. 6b. The red-shift for the long-time deposition sample indicates growth of ZnO crystallites. The absorption is higher with increasing ZnO deposition time, which can be ascribed to the larger amount of deposited ZnO. The absorption edge of pure CdS starts around 530 nm (Fig. 6a), which agrees with the intercept of 2.36 eV, as shown in the inset of Fig. 6b. The absorption spectrum of ZnO/CdS nanoarrays with 3 min CdS deposition is similar to that of bare ZnO nanorods, which is due to too small amount of existing CdS. The visible light absorption for samples with CdS increases with CdS deposition duration. The absorption spectrum of ZnO/CdS nanoarrays with 40 min CdS deposition looks similar to that of the pure CdS deposited for 2 h, showing that the CdS-coating is predominantly responsible for the observed optical performance. The spectra of the samples with CdS deposition for 10 min and 20 min are located between those with CdS deposition for 3 min and 40 min, and the observable absorption edges of CdS in ZnO/CdS nanoarrays start at approximately 515 nm (Fig. 6a), with a bandgap of 2.41 eV (see inset in Fig. 6b). Compared to the pure CdS sample, the blue-shift of CdS absorption in ZnO/CdS nanoarrays with the short CdS deposition duration is thus indicative of small CdS nanoparticles subjected to strain during growth on ZnO. The interesting observation is the crossing at ~390 nm of the two spectra of ZnO/CdS nanoarrays with CdS deposition for 10 min and 20 min. The absorption of ZnO is stronger in the former sample than in the latter, while the absorption of CdS shows the inverse order. This can be attributed to the increased deposition of CdS and the increased etching of ZnO with the continuous deposition of CdS, which agrees with the results from XRD, Raman spectroscopy, and EDX.

The PL spectrum (Fig. 7) of ZnO nanorods (on FTO) shows two luminescent bands under the excitation wavelength of 350 nm. One is the UV emission peak, which corresponds to the near band-edge emission, and the other is the green emission peak [32–34]. The green emission nearly disappears at the excitation wavelength of 325 nm, while at the excitation wavelengths above 350 nm the UV emission peak disappears. The PL spectrum of CdS-coated ZnO nanorods also show two luminescence bands under the excitation wavelength of 350 nm, both strongly enhanced compared to bare ZnO. No additional fluorescence band from CdS could be directly observed at different excitation wavelengths [19,32,35]. The PL spectra show that incident light excites charge-carriers on CdS, which subsequently transfer to ZnO followed by radiative decay.

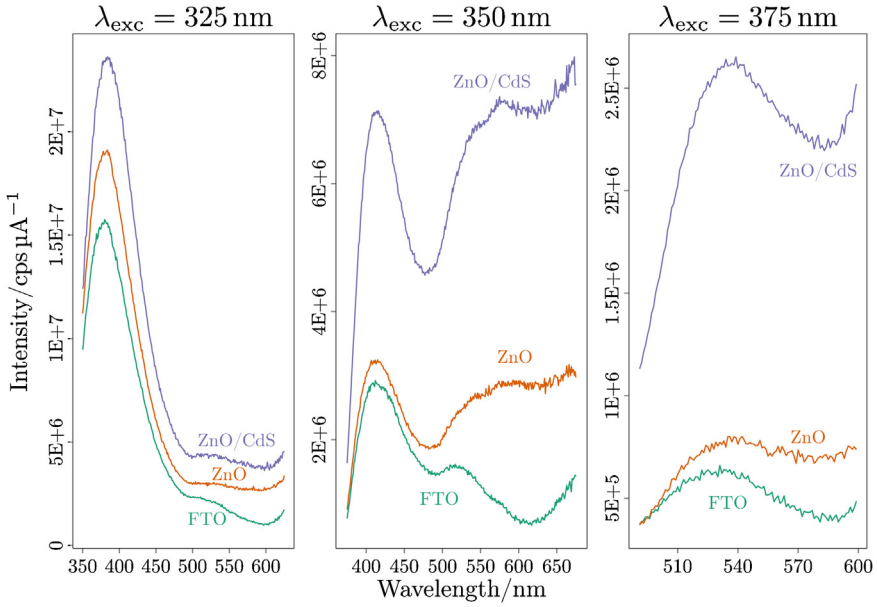

Fig. 7. Photoluminescence spectra of FTO, ZnO on FTO, and ZnO/CdS on FTO at different excitation wavelengths (325 nm, 350 nm, and 375 nm).

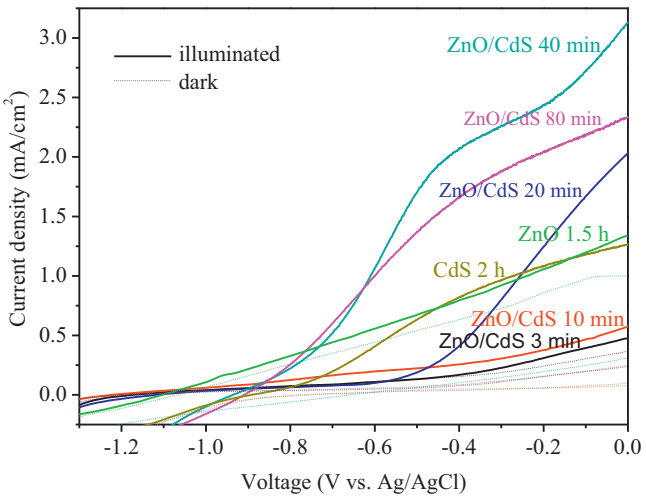

Fig. 8. *J–V* curve of ZnO/CdS nanoarrays with different CdS growth time from 3 min to 80 min (denominated as ZnO/CdS *x* min), ZnO nanorods electrodeposited for 1.5 h with initial pulse (ZnO 1.5 h), and CdS deposited on FTO for 2 h (CdS 2 h) in the dark (broken lines) and under simulated solar illumination (solid lines).

3.5. Photoelectrochemical properties

Fig. 8 presents the results from *J–V* measurement of some prepared samples. The dark current of bare ZnO is high, showing ohmic characteristic with varying bias. The high dark current might be due to incomplete coverage of these ZnO nanorods on FTO. However, the contribution from some chemical process on ZnO to this dark current cannot be ruled out. The photocurrent of pure ZnO is barely larger than its dark current, which is due to the poor visible light response of ZnO. The high dark current and the low photo-sensitivity (i.e. the photocurrent-to-dark current contrast ratio) of bare ZnO may be also related to the oxygen vacancies [36]. CdS-coated ZnO samples show a decreased dark current, which may result from the poor conductivity of CdS and its covering of ZnO nanorods and exposed FTO substrate. But they show an increased photo-sensitivity, which is due to the visible-light sensitivity of CdS. The extent of the decreasing dark current and the increasing photo sensitivity largely depends on the amount of CdS deposited. For example, the sample prepared by a 3 min CdS deposition on ZnO nanorods also has a low photo-sensitivity and a high dark current, which can be ascribed to too small coverage of CdS. This is in agreement with the result from the optical absorption measurement. With increasing CdS deposition time, the photocurrent of ZnO/CdS starts to increase drastically. The best performance is observed for the sample with 40 min CdS deposition. The short-circuit current density (J_{sc}) of this sample is 3.31 mA/cm^2 under illumination, while the open-circuit voltage (V_{oc}, *V* vs. Ag/AgCl) is −0.94 V. The photoelectrochemical performance does not improve by increasing the CdS deposition time to 80 min, since a thick CdS layer extends the migration distance of the photogenerated electrons to the ZnO layer, and thus increases the possibility for the recombination of electrons and holes. Furthermore, the separated CdS clusters resulted from too high deposition cannot contribute to the photoelectrochemical performance.

The photoelectrochemical test demonstrates that ZnO/CdS nanoarrays can give higher performance than bare ZnO nanorods and CdS nanoparticles. In ZnO/CdS nanoarray photoanodes, CdS absorbs the visible light to generate electrons and holes, and the function of ZnO is mainly to transfer electrons from CdS to the external circuit. The amount of deposited CdS (and etched ZnO) influences the photoelectrochemical properties of the ZnO/CdS nanoarrays. Therefore, the optimal deposition and growth time of CdS is the key factor that determines the photoelectrochemical properties of the ZnO/CdS nanoarrays. The presented photocurrent can possibly be further enhanced by more coverage of ZnO/CdS nanoarrays on FTO, which is presently under investigation.

3.6. Photocatalytic properties

The photocatalytic activity of our ZnO/CdS nanoarrays was evaluated by the degradation of EBT and compared with bare ZnO nanorods. In Fig. 9a, bare ZnO has little photocatalytic activity (less than 5% EBT degradation) under visible light irradiation, due to its weak response to visible light. With increasing CdS deposition time, the photocatalytic activity of ZnO/CdS starts to increase markedly. The best photocatalytic activity is observed for the sample with 40 min CdS deposition, after which the photocatalytic activity starts decreasing with further CdS deposition. The degradation of EBT followed apparent zero-order or first-order kinetics, depending on the sample used. Highly efficient degradation showed pseudo first-order kinetics, while pseudo zero-order kinetics was observed in slower degradation. In difference from the results of the photoelectrochemical test, the ZnO/CdS 20 min sample shows comparable photocatalytic activity to the ZnO/CdS 40 min sample (see Fig. 9a). This can be explained by the different roles of ZnO in these two tests. In the photoelectrochemical test, ZnO helps to separate the photogenerated electrons and holes by transferring the electrons to the current collector (FTO); while in the photocatalytic test, besides the oxidation of EBT by the photogenerated holes in CdS (Eq. (17)), ZnO can attract the photogenerated electrons from CdS, reduce dissolved molecular oxygen O_2 to the superoxide radical anion $O_2^{\bullet -}$, and then produce hydroxyl radical OH$^\bullet$, which is a strong oxidant that can degrade EBT. The conjugated system in EBT is easily destroyed, while the aromatic rings could also be broken down by hydroxyl radical OH$^\bullet$ [37]. This mechanism can be described with Eqs. (11)–(16) below.

$$ZnO/CdS + h\nu \rightarrow h_{CdS}^{+} + e_{ZnO}^{-} \quad (11)$$

$$e_{ZnO}^{-} + O_2 \rightarrow O_2^{\bullet -} \quad (12)$$

$$O_2^{\bullet -} + H_2O \rightarrow HO_2^{\bullet} + OH^{-} \quad (13)$$

$$HO_2^{\bullet} + H_2O \rightarrow H_2O_2 + OH^{\bullet} \quad (14)$$

$$H_2O_2 \rightarrow 2OH^{\bullet} \quad (15)$$

$$EBT + OH^{\bullet} \rightarrow CO_2 + H_2O \quad (16)$$

$$EBT + h_{CdS}^{+} \rightarrow CO_2 + H_2O \quad (17)$$

The incomplete coverage of ZnO surface is thus beneficial to the decomposition of EBT, since the electrons in ZnO also participate in photocatalytic reactions. Therefore the optimum loading amount of CdS for the photocatalytic test might be smaller than that for the photoelectrochemical test. We observed photocorrosion starting after 2 h photocatalytic reaction, which is a common problem for all metal sulfides. It should be noted that no sacrificial agents (hole scavengers, such as alcohols or sulfide/sulfite ions) were used in the current photocatalytic experiments. Normally, the photo-corrosion stability and photocatalytic efficiency of CdS can be improved by adding sacrificial agents in solution. Therefore, it is still possible to enhance the photocatalytic activity of these prepared nanocomposites (should sacrificial agents be employed). An interesting next step is to separate the light absorber from the photocatalytically active sites with e.g. a thin protective layer of a wide band-gap metaloxide [38] by atomic layer deposition. This would add the additional advantages of limiting any undesired photocorrosion and introducing more photocatalytically active sites, meanwhile complete coverage of exposed areas of the FTO would also improve the photocatalytic efficiency.

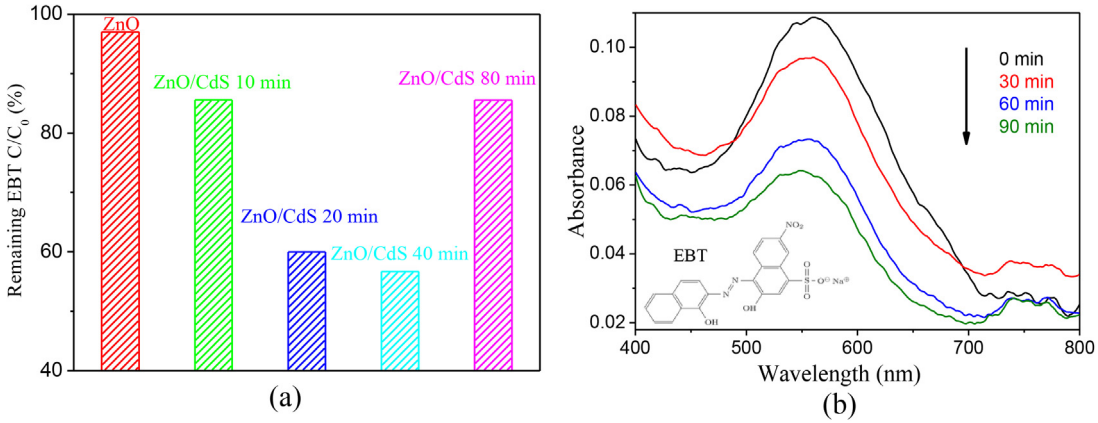

Fig. 9. (a) EBT contents remaining in the solution after 90 min photocatalytic degradation under LED light irradiation (450 nm). (b) Absorption spectra of the photocatalytically degraded EBT solutions with the sample ZnO/CdS 40 min. Inset: the structural formula of EBT.

4. Conclusions

We have demonstrated a simple route to obtain ZnO/CdS nanoarrays by the combination of electrodeposition and chemical deposition. The initial pulse was shown to be important for a homogeneously distributed seed layer of ZnO for a subsequent growth of ZnO nanorods. The nanorod morphology is maintained after coating CdS outside ZnO. The ZnO/CdS nanoarrays with suitable composition show much improved photoelectrochemical and photocatalytic performances compared to bare ZnO under visible light irradiation, due to the efficient charge carrier separation between CdS and ZnO. Further optimization and surface engineering of the prepared ZnO/CdS nanoarrays can possibly be used to fabricate cheap solar-energy conversion devices. As the fabrication method is general and applicable to a wide range of similar hybrids as photocatalysts and photoanodes, and it can thus also be extended to other materials systems.

Acknowledgements

The authors thank Ångpanneföreningen's Foundation for Research and Development (Ref. nr 09-370), Carl Tryggers foundation, and the Swedish Association of Graduate Engineers for their financial support. C.L. gratefully acknowledges the financial support of Alistore (Erasmus Mundus). The authors would like to thank Gabriel Oltean for valuable discussions regarding the electrodeposition of ZnO.

References

[1] K. Keis, C. Bauer, G. Boschloo, A. Hagfeldt, K. Westermark, H. Rensmo, H. Siegbahn, Journal of Photochemistry and Photobiology a-Chemistry 148 (2002) 57–64.
[2] J. Zhu, D. Chakarov, M. Zäch, in: L. Zang (Ed.), Springer London, 2011, pp. 441–486.
[3] Y. Tak, S.J. Hong, J.S. Lee, K. Yong, Crystal Growth and Design 9 (2009) 2627–2632.
[4] X.-J. Wu, F. Zhu, C. Mu, Y. Liang, L. Xu, Q. Chen, R. Chen, D. Xu, Coordination Chemistry Reviews 254 (2010) 1135–1150.
[5] Z. Chen, Y. Tang, L. Zhang, L. Luo, Electrochimica Acta 51 (2006) 5870–5875.
[6] L. Xu, Y. Guo, Q. Liao, J. Zhang, D. Xu, The Journal of Physical Chemistry B 109 (2005) 13519–13522.
[7] J. Yang, G. Liu, J. Lu, Y. Qiu, S. Yang, Applied Physics Letters 90 (2007) 103109.
[8] J. Yang, Y. Qiu, S. Yang, Crystal Growth and Design 7 (2007) 2562–2567.
[9] M.J. Zheng, L.D. Zhang, G.H. Li, W.Z. Shen, Chemical Physics Letters 363 (2002) 123–128.
[10] L. Xu, Q. Liao, J. Zhang, X. Ai, D. Xu, The Journal of Physical Chemistry C 111 (2007) 4549–4552.
[11] W. Jih-Jen, C. Ru-Chun, L. Chih-Cheng, Journal of The Electrochemical Society 155 (2008), D771-D776D776.
[12] R. Liu, A.A. Vertegel, E.W. Bohannan, T.A. Sorenson, J.A. Switzer, Chemistry of Materials 13 (2001) 508–512.
[13] T. Pauporte, D. Lincot, Electrochimica Acta 45 (2000) 3345–3353.
[14] J. Zhu, M. Zach, Current Opinion in Colloid & Interface Science 14 (2009) 260–269.
[15] S. Sakthivel, S.U. Geissen, D.W. Bahnemann, V. Murugesan, A. Vogelpohl, Journal of Photochemistry and Photobiology A: Chemistry 148 (2002) 283–293.
[16] X.P. Qi, G.W. She, Y.Y. Liu, L.X. Mu, W.S. Shi, Chemical Communications 48 (2012) 242–244.
[17] Y. Tak, S.J. Hong, J.S. Lee, K. Yong, Journal of Materials Chemistry 19 (2009) 5945–5951.
[18] Y. Tak, H. Kim, D. Lee, K. Yong, Chemical Communications (2008) 4585–4587.
[19] P. Kundu, P.A. Deshpande, G. Madras, N. Ravishankar, Journal of Materials Chemistry 21 (2011) 4209–4216.
[20] S. Peulon, D. Lincot, Journal of The Electrochemical Society 145 (1998) 864–874.
[21] D.S. Boyle, A. Bayer, M.R. Heinrich, O. Robbe, P. O'Brien, Thin Solid Films 361–362 (2000) 150–154.
[22] A.I. Oliva, R. Castro-Rodrıǧuez, O. Ceh, P. Bartolo-Pérez, F. Caballero-Briones, V.C. Sosa, Applied Surface Science 148 (1999) 42–49.
[23] K. Senthil, D. Mangalaraj, S.K. Narayandass, Applied Surface Science 169–170 (2001) 476–479.
[24] Y.F. Zhu, W.Z. Shen, Applied Surface Science 256 (2010) 7472–7477.
[25] D. Raymand, T.J. Jacobsson, K. Hermansson, T. Edvinsson, The Journal of Physical Chemistry C 116 (2012) 6893–6901.
[26] H. Sun, Y. Chen, X. Li, W. Li, Y. Xie, B. Liu, X. Zhang, Solid State Communications 150 (2010) 820–823.
[27] S. Mishra, A. Ingale, U.N. Roy, A. Gupta, Thin Solid Films 516 (2007) 91–98.
[28] T.B. Elliot, Trends in Semiconductor Research, Nova Science Publishers, New York, 2005.
[29] O. Manasreh, Introduction to Nanomaterials and Devices, John Wiley & Sons, New Jersey, 2011.
[30] M.D. Archer, A.J. Nozik, Nanostructured and Photoelectrochemical Systems for Solar Photon Conversion, Imperial College Press, London, 2008.
[31] U.K. Mishra, J. Singh, Semiconductor Device Physics and Design, Springer, Dordrecht, 2007.
[32] T. Gao, Q. Li, T. Wang, Chemistry of Materials 17 (2005) 887–892.
[33] B.Y. Geng, G.Z. Wang, Z. Jiang, T. Xie, S.H. Sun, G.W. Meng, L.D. Zhang, Applied Physics Letters 82 (2003) 4791–4793.
[34] S. Khanchandani, S. Kundu, A. Patra, A.K. Ganguli, The Journal of Physical Chemistry C 116 (2012) 23653–23662.
[35] N.A. Dhas, A. Gedanken, Applied Physics Letters 72 (1998) 2514–2516.
[36] J.M. Wu, Y.R. Chen, Journal of Physical Chemistry C 115 (2011) 2235–2243.
[37] J. Zhu, J. Zhang, F. Chen, K. Iino, M. Anpo, Topics in Catalysis 35 (2005) 261–268.
[38] A. Paracchino, V. Laporte, K. Sivula, M. Grätzel, E. Thimsen, Nature Materials 10 (2011) 456–461.